

pubs.acs.org/cm Article

Hydrothermal Synthesis and Solid-State Laser Refrigeration of Ytterbium-Doped Potassium-Lutetium-Fluoride (KLF) Microcrystals

Xiaojing Xia, Anupum Pant, Xuezhe Zhou, Elena A. Dobretsova, Alexander B. Bard, Matthew B. Lim, Joo Yeon D. Roh, Daniel R. Gamelin, and Peter J. Pauzauskie*

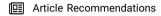


Cite This: Chem. Mater. 2021, 33, 4417-4424



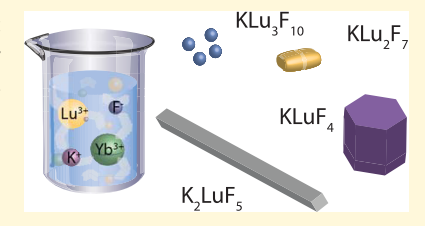
ACCESS

Metrics & More



SI Supporting Information

ABSTRACT: Hydrothermal methods are used for the first time to synthesize distinct crystallographic stoichiometries within the potassium-lutetium-fluoride phase diagram for applications in solid-state laser refrigeration. Four crystalline phases were synthesized hydrothermally and doped with 10% Yb(III) ions, namely, orthorhombic K_2LuF_5 (space group Pnma), trigonal $KLuF_4$ (space group $P3_1$ 21), orthorhombic KLu_2F_7 (space group $Pna2_1$), and cubic KLu_3F_{10} (space group Fm3m), with each phase exhibiting unique microcrystalline morphologies. Among the four phases, the most significant cooling was observed for the $KLuF_4$ phase, which showed an overall refrigeration of 8.6 ± 2.1 K below



room temperature. Laser refrigeration for $KLuF_4$ was measured by observing both the eigenfrequencies of optomechanical cantilevers in vacuum and also the Brownian dynamics of optically trapped microcrystals in water. Cooling was also observed for the first time for the K_2LuF_5 phase in vacuum based on measurements of the mean luminescence wavelength of Yb(III) ions. Cooling was not observed with the other two phases.

■ INTRODUCTION

Rare-earth (RE)-doped materials have been investigated for use in a wide range of luminescent upconversion/downconversion applications including bioimaging, photocatalysis, solar cells,^{3–5} telecommunications,⁶ quantum information science, and solid-state laser refrigeration. Laser cooling in solids arises from the extraction of heat from a material based on spontaneous, anti-Stokes luminescence that follows the thermalization of optically excited ions. Phonons provide the energy required for the emission of anti-Stokes photons. The anti-Stokes photons that escape from the solid transfer thermal energy out of the material. Laser cooling through anti-Stokes luminescence was first proposed for metal atoms in the gas phase by Pringsheim in 1929.9 Later, in 1950, Kastler proposed the use of RE ions for anti-Stokes laser refrigeration due to their high quantum efficiencies. 10 The first experimental demonstration of solid-state laser cooling involved a Ybdoped ZBLANP glass material in 1995. 11 To date, net cooling has been observed in a wide variety of glasses 11-16 and crystals^{15,17-21} doped with RE ions.

Currently, the development of new laser refrigeration materials is focused primarily on RE-doped crystals grown using the Czochralski process²² due to stringent requirements for low background absorption and near-unity radiative quantum efficiencies. A Yb-doped lithium-yttrium-fluoride (LiYF₄) crystal grown using the Czochralski approach has been reported to cool to cryogenic temperatures (91 K) through a vibration-free anti-Stokes photoluminescence process.²³ Recently, both lithium-yttrium-fluoride²⁴ and

sodium-yttrium-fluoride materials²⁵ were reported to achieve internal laser refrigeration in aqueous solution.

To date, potassium-based fluoride materials have been studied less extensively than their Na and Li counterparts due in part to the complexity of potassium-RE-fluoride phase diagrams.²⁶ In contrast with lithium yttrium fluoride, which is known to have only one tetragonal phase (LiYF₄), potassium-RE-fluorides have at least five stable crystallographic phases including K_3REF_6 , K_2REF_5 , $KREF_4$, KRE_2F_7 , and KRE_3F_{10} . This multitude of phases can be represented more intuitively by the stoichiometric formula $(KF)_x \cdot (REF_3)_y$ resulting in different crystal structures for different values of "x and "y". This variety of crystal structures provides a rich array of potential luminescent materials. The diversity of potassium-RE-fluoride phases also has attracted recent theoretical interest³⁰ for potential applications in laser refrigeration. However, to the best of the authors' knowledge, there is only a single experimental report for laser cooling of KYF4 materials within the potassium-RE-fluoride phase diagram² using bulk crystals grown using the Czochralski process. The relative lack of data for potassium-RE-fluoride materials stems from challenges of growing bulk single crystals with welldefined stoichiometries using classical Czochralski or Bridg-

Received: February 4, 2021 Revised: May 20, 2021 Published: June 6, 2021





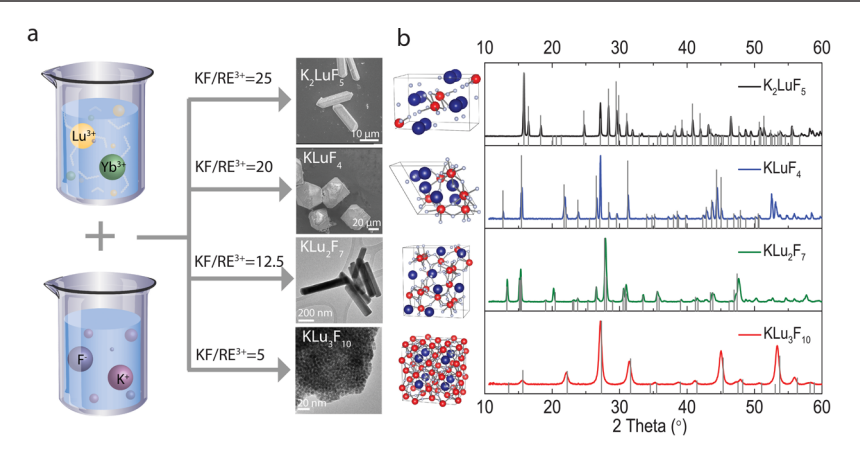


Figure 1. (a) Microscope images of KLF crystals synthesized with various molar ratios of KF to RE³⁺ in the starting solutions. The counteranion is NO_3^- for all syntheses. (b) XRD patterns of KLF samples synthesized with KF/RE = 25, 20, 12.5, 5 (from top to bottom) and the corresponding lattice structures. The blue, red, and gray atoms represent potassium, lutetium, and fluorine, respectively. The standard data of K_2LuF_5 (PDF Card 04-005-6013), KLuF₄ (PDF 04-019-4298), and KYb₂F₇ (PDF 00-027-0459), KLu₃F₁₀ (PDF 04-002-4130) are given as references. KLu₂F₇ is not available in the database. Its XRD peaks are shifted slightly to larger angles with respect to the KYb₂F₇ reference because the Lu³⁺ ionic radius (0.861 Å) is slightly smaller than that of Yb³⁺ (0.868 Å). All samples are doped with 10%Yb³⁺.

Table 1. Crystallographic Information for K-Lu-F Crystals and Other Laser Cooling Materials

sample	crystal system	space group	Yb ³⁺ site symmetry	max phonon energy	centro/noncentro
K_2LuF_5	orthorhombic	Pnma	C_2	506 cm ⁻¹	centrosymmetric
KLuF ₄	trigonal	$P3_{121}$	C_1	508 cm ⁻¹	noncentrosymmetric
KLu_2F_7	orthorhombic	$Pna2_1$	C_2 , C_1	529 cm^{-1}	noncentrosymmetric
KLu_3F_{10}	cubic	$Fm\overline{3}m$	$C_{4 u}$	509 cm^{-1}	centrosymmetric
LiYF ₄ ¹⁹	tetragonal	$I4_1/a$	S_4	450 cm ⁻¹ 19	centrosymmetric
LiLuF ₄ ^{21,37}	tetragonal	$I4_1/a$	S_4	375 cm^{-1}	centrosymmetric
KYF_4^{20}	trigonal	$P3_1$	C_2 , C_1	350 cm ⁻¹	noncentrosymmetric
β -NaYF $_4^{38}$	hexagonal	$P\overline{6}^a$	$C_{3 u}$	360 cm ^{-1 39}	noncentrosymmetric

 $^{a}P6_{3}/m$ and $P\overline{6}2m$ also exist. 40

man bulk crystal growth techniques. Although the investigation of potassium-RE-fluoride systems started over half a century ago,³¹ there are no reports in the scientific literature investigating solid-state laser cooling with the K-RE-F material growth using hydrothermal synthesis.

This work is the first systematic study of K-RE-F as laser refrigeration host materials. We overcome the challenges of growing laser cooling crystals with the Czochralski method through the use of a novel hydrothermal chemical synthesis approach. We demonstrate the rapid, low-cost hydrothermal synthesis of four $(KF)_x$ · $(REF_3)_y$ crystallographic phases $(KLu_3F_{10}, KLu_2F_7, KLuF_4, \text{ and } K_2LuF_5)$ with well-defined stoichiometries. The common host element yttrium is replaced with lutetium, as the close match in cation size between Lu^{3+} (861 pm) and the dopant ion Yb^{3+} (868 pm) 32 enables improved crystal quality. The KLu_3F_{10} , KLu_2F_7 , and K_2LuF_5 phases have not been reported to be grown using bulk techniques.

Each crystalline phase exhibits a distinct morphology, with crystallite sizes ranging from nanometers to hundreds of micrometers. Photoluminescence spectra and lifetimes of the four crystalline phases were characterized based on the point-group symmetry of trivalent cations in each phase. The laser refrigeration performance of each phase was quantified via (1) measuring the temperature-dependent eigenfrequency of optomechanical cantilever devices in vacuum, (2) observing the Brownian dynamics of microcrystals optically trapped in water, (3) from measuring the mean luminescence wavelength of Yb(III) ions. (3) Micron-scale KLuF₄ shows the

most significant cooling among all four crystalline phases investigated, with minimum temperatures of $8.6 \pm 2.1~\mathrm{K}$ below room temperature. Cooling was also observed for the first time in the $\mathrm{K_2LuF_5}$ phase in vacuum. This material platform is promising for future use in micron-scale radiation-balanced lasers, in which cooling by anti-Stokes luminescence compensates for the heat generated during lasing. ³⁵

■ RESULTS AND DISCUSSION

Rapid, low-cost hydrothermal methods were used to grow Ybdoped (KF)_x·(LuF₃)_v crystals. Four phases, KLu₃F₁₀, KLu₂F₇, KLuF₄, and K₂LuF₅, were successfully synthesized by varying the concentration of the KF precursor (see the Supporting Information (SI) for details). Figure 1 shows the morphologies and powder X-ray diffraction (XRD) patterns of these four phases at different KF/RE³⁺ ratios from 5:1 to 25:1. The assynthesized samples shown in Figure 1 exhibit distinct shapes and lattice structures. Under otherwise identical reaction conditions, increasing the KF/RE³⁺ ratio increases the sizes of the resulting particles. Furthermore, the characteristic morphology of the particles changes, as shown in Figure 1. The K₃LuF₆ phase was not observed using hydrothermal synthesis, even with a KF/RE³⁺ ratio as high as 60. This observation is consistent with previous experiments that show only four phases of $(KF)_x \cdot (YbF_3)_y$ crystals in hydrothermal synthesis. 36 In contrast with the nonstoichiometric sodium-REfluoride system,²⁸ to the best of our knowledge, the potassium-RE-fluoride phases we report are stoichiometric. The diffraction patterns of these products prepared with different

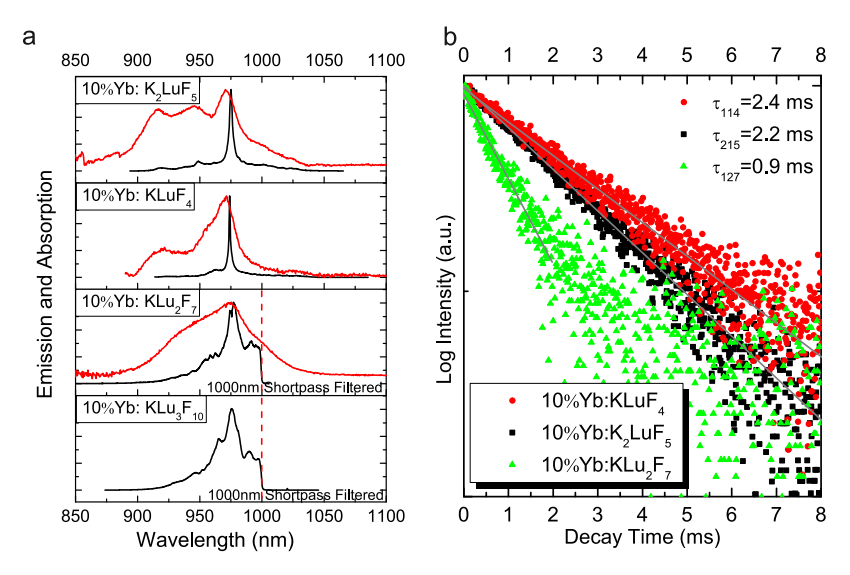


Figure 2. (a) Room-temperature PL (black) and absorption (red) spectra probing the Yb(III) ${}^2F_{5/2} \rightarrow {}^2F_{7/2}$ electronic transition of 10% Yb:K2LuF₅, 10%Yb:KLuF₄, 10%Yb:KLu₂F₇, and 10%Yb:KLu₃F₁₀ under a 1020 nm laser excitation. (b) PL decay profiles of the Yb(III) ${}^2F_{5/2} \rightarrow {}^2F_{7/2}$ transitions of 10%Yb:K2LuF₅, 10%Yb:KLuF₄, and 10%Yb:KLu₂F₇. The lifetimes for each sample are obtained from single exponential fitting.

KF/RE ratios can be indexed to orthorhombic K₂LuF₅, trigonal KLuF₄, orthorhombic KLu₂F₇, and cubic KLu₃F₁₀. More details of these four crystallographic phases are listed in Table 1. Among these phases, KLisare provided as well for comparison.

Control over the crystallographic phase and morphology requires a detailed understanding of the thermodynamics and kinetics underlying crystal growth. Growth of KF-rich crystal phases involves the formation of lower KF/LuF₃ phases at early stages of crystal growth. For example, KLu₃F₁₀, KLu₂F₇, and KLuF4 are formed during the first hour of the K2LuF5 growth (Figures S1-S5). Among the various potassiumlutetium-fluoride (KLF) crystal systems, K2LuF5 is a good candidate to study crystallization kinetics in nanometer and micron-sized scales because of its rodlike morphology and high growth speed. The growth velocity of K₂LuF₅ is at least 0.77 μ m/min along the growth direction and 0.10 μ m/min perpendicular to the growth direction in the first hour (Figure S6). We also observed that the Yb³⁺ concentration controls the length of K₂LuF₅ rods, with that length increasing with higher Yb³⁺ concentrations (Figure S7). While the crystal length is obviously affected, the crystal width does not change significantly. Statistics for K2LuF5 crystal length and width are illustrated in Figure S7 with different Yb3+ doping levels. Differences in the morphology and aspect ratio for various lanthanide hydroxides also have been reported, 41 in which the surface energy has been proposed to control the growth rate and therefore the aspect ratio. However, when there is 100% Yb3+ in the crystal, i.e., K2YbF5, the crystal length is only around 20 um, much shorter than expected. A detailed study of the factors that affect crystal length remains a subject for future

Figure 2 summarizes the photoluminescence (PL) of 10% Yb: K_2LuF_5 , 10%Yb: $KLuF_4$, 10%Yb: KLu_2F_7 , and 10%Yb:- KLu_3F_{10} upon a 1020 nm laser excitation. Yb³⁺ in the KLF host matrix has its $^2F_{7/2}$ ground-state and $^2F_{5/2}$ excited-state manifolds split into Stark levels due to the electrostatic crystal field. If the Yb³⁺ point symmetry is lower than cubic (O, O_h , T_d), the $^2F_{5/2}$ and $^2F_{7/2}$ states split into 3 and 4 Kramers doubly degenerate Stark levels, respectively; otherwise, they split into

2 and 3 crystal-field levels, respectively.³⁰ The Kramers degeneracies are only lifted under an applied magnetic field. The Stark multiplet structure of excited and ground states determines the relaxation channels resulting in Stokes and anti-Stokes emissions.⁴² In Figure 2, the emission spectra of each sample are distinct due to differences in Yb3+ site symmetries. The full emission spectra of Yb³⁺ $^2F_{5/2} \rightarrow ^2F_{7/2}$ transitions for 10%Yb:K₂LuF₅ and 10%Yb:KLuF₄ single crystals were recorded by using time-gated spectroscopy. Although there are 12 allowed transitions, only one dominant peak around 974 nm was observed. For the 10%Yb:KLuF₄ sample, the full width at half-maximum (FWHM) of the primary peak is less than 2 nm without any further processing of the crystal. A side peak around 1030 nm is reported in structurally similar Yb:KYF₄, ²⁰ but we did not observe such peaks in our detector range. Besides the intense emission at 974 nm, both 10%Yb:K₂LuF₅ and 10%Yb:KLuF₄ have luminescence lifetimes longer than 2 ms (Figure 2b). For 10%Yb:KLu₂F₇ and 10%Yb:KLu₃F₁₀, the measured Yb3+ lifetimes are short compared to the other samples; 10%Yb:KLu₂F₇ has a luminescence lifetime of 874 μ s, and for 10%Yb:KLu₃F₁₀, the luminescence lifetime was shorter than the 100 μ s resolution of our detector. Due to the relatively short luminescence lifetime, the time-gated method for a full-range emission spectrum did not work well for the $10\%Yb:KLu_2F_7$ and $10\%Yb:KLu_3F_{10}$ samples. Instead, a 1000nm short-pass filter was applied to block the laser line. The spectra below 1000 nm were recorded for 10%Yb:KLu₂F₇ and 10%Yb:KLu₃F₁₀. According to Figure 2a, the PL features from these two crystalline phases are much broader than those of the previous two phases. Such differences in spectral line shape result from differences in the local symmetry and strength of the electrostatic crystal field, 43 as well as from differences in inhomogeneous broadening.

The lifetime we measured is the inverse of the total decay rate constant, $W = W_{\rm r} + W_{\rm nr}$, which has radiative $(W_{\rm r})$ and nonradiative $(W_{\rm nr})$ components. The radiative decay rate constant reflects the oscillator strength of the same transition and is related to the local symmetry of the Yb³⁺, whereas the nonradiative decay rate constant is affected by the lattice phonon energies, dopant concentrations, and defects with

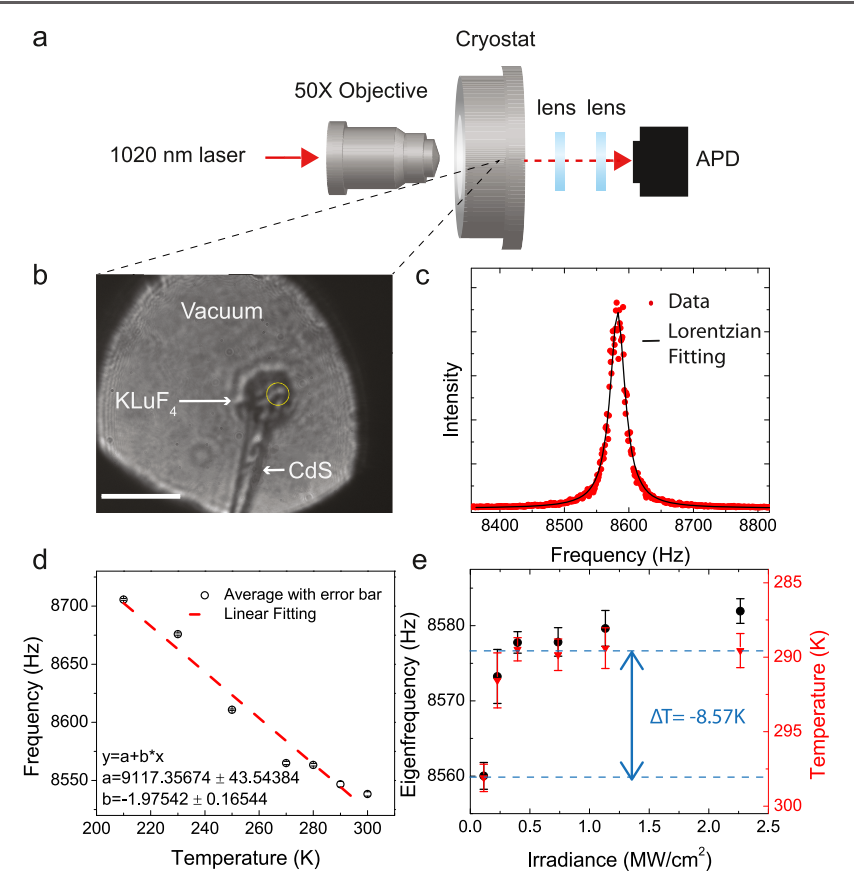


Figure 3. (a) Schematic of the experimental setup for the eigenfrequency measurement. (b) Microscope image of a CdSNR with a 10%Yb:KLuF₄ crystal (scale bar: $10 \mu m$). (c) Representative Lorentzian fitting curve (black) of the eigenfrequency peak in the Fourier-transformed signal from the avalanche photodiode (APD) (red). (d) Frequency vs. temperature calibration of the CdSNR + crystal cantilever. Black open circles: average frequency of six measurements. The error bar represents 1 standard deviation. Red: linear least-squares fit. The eigenfrequency decreases when increasing the temperature. (e) Frequencies measured (black) at various irradiances and the frequencies after subtracting the effect of optical trapping (red). The subtracted frequencies are used to fit the temperature.

high-energy vibrational modes. Because W_{nr} is temperaturedependent, the PL lifetime could be used to probe the local temperature at the nanometer scale.⁴⁴ Radiative and nonradiative relaxation mechanisms can be modified by the local symmetry of the host lattice and by crystal size, respectively. 45 Here, the radiative decay rate constant cannot be estimated without more detailed spectroscopic data. Some potential reasons for the lifetime difference can be ruled out, such as impurities inside the crystal, energy transfer processes that depend on dopant concentration, and lattice phonon energies. In our study, the starting materials, synthesis method, and Yb3+-doping concentrations of these KLF crystals are all the same. Instead, the long emission lifetimes of 10%Yb:K2LuF5 and 10%Yb:KLuF4 are attributed to the small nonradiative decay rates and also potential radiation trapping in these largesized crystals. 46 Surface defects are one of the main causes of nonradiative decay for these fluoride crystals as the fluoride phonon energy is low. FTIR spectra indicating the highest vibrational mode of each crystalline phase are shown in Figure S8. A large crystal volume lowers the surface-to-volume ratio and thus decreases nonradiative decay.⁴⁷ Yb³⁺ ions exhibit significant overlap between their absorption and emission spectra. Therefore, the reabsorption of emission is nonnegligible in crystals with characteristic dimensions on the order of 100 micrometers. This can result in measured luminescence lifetimes as much as 30% longer than the expected value. 48 In this approximation, the corrected lifetimes

of 10%Yb:K₂LuF₅ and 10%Yb:KLuF₄ are 1.68 and 1.86 ms, respectively. The sharp and intense emission at 974 nm for these two samples is possibly the result of reabsorption. Such luminescence reabsorption is an important factor for laser media, as it can be used as an additional pumping source, recycling energy that would otherwise be lost as spontaneous luminescence. Reabsorption can therefore have a substantial influence on laser efficiency. However, such reabsorption processes can cause heat if the spontaneous photon finds a parasitic impurity through those many reabsorptions in the crystals, which requires high purity of the materials. If laser refrigeration can be achieved in these crystals, they could be promising candidates for radiation-balanced microlasers.

To evaluate the laser refrigeration properties of these assynthesized crystals, the crystals were transferred onto a cadmium sulfide nanoribbon cantilever (CdSNR) with low NIR absorption to measure the temperature via the cantilever's optomechanical eigenfrequency. As the temperature decreases, the Young's modulus of the CdSNR increases and thus the eigenfrequency increases as well. The experimental setup and an optical micrograph of a ground 10%Yb:KLuF4 crystal on the CdSNR in a vacuum cryostat are shown in Figure 3a,3b. Details for device fabrication are discussed further in the Experimental Section. Figure 3c shows a representative eigenfrequency spectrum fit numerically with a Lorentzian. The eigenfrequencies at various temperatures were measured and linearly fit (Figure 3d) with a slope of 2 Hz/K

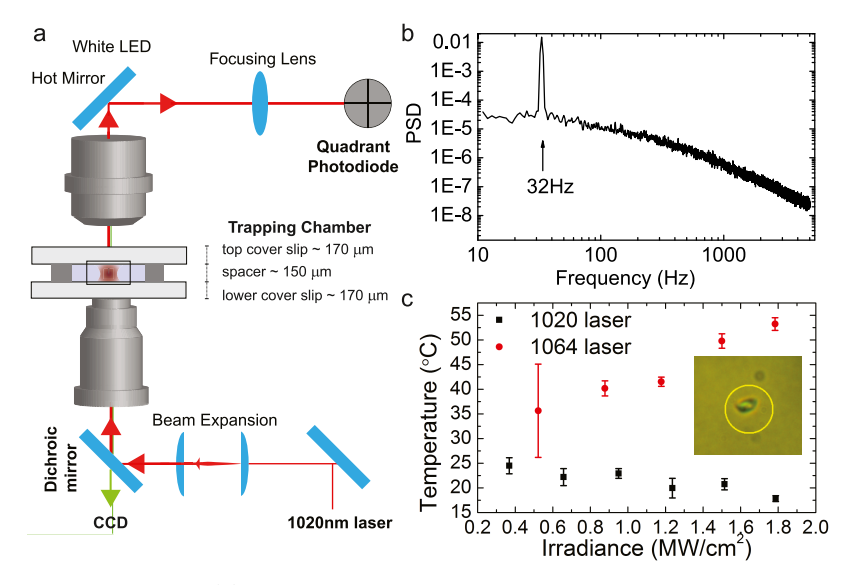


Figure 4. (a) Schematic of laser trapping setup. (b) Representative power spectrum of a trapped particle undergoing Brownian motion in water with a 32 Hz oscillation. (c) Temperature of a 10%Yb:KLuF₄ crystal trapped by a 1020 nm laser and by a 1064 nm laser in water.

for calibration of subsequent laser refrigeration experiments. When excited by a 1020 nm laser, the eigenfrequency was observed to increase with increasing laser irradiance, indicating net cooling of the cantilever. The eigenfrequency blue-shifts 22 ± 3 Hz at the maximum irradiance (Figure 3e).

The eigenfrequency of the cantilever depends not only on its temperature-dependent Young's modulus but also on potential laser trapping forces, where the laser trap can be modeled as a Hookean spring located at the end of the cantilever. With increased laser irradiance, the spring constant increases and thus the cantilever eigenfrequency increases. The red data in Figure 3e show that after subtracting the increase in eigenfrequency related to optical trapping, the blue shift due to the temperature change is 17 ± 4 Hz (see Figure S11 and the discussion in the Supporting Information). According to the temperature calibration, this shift indicates a temperature decrease of 8.6 ± 2.1 K (Figure 3e) for 10%Yb:KLuF₄. Laser refrigeration is not observed in other crystal phases (see the Supporting Information).

In addition to laser refrigeration in vacuum, we observed laser refrigeration of ground 10%Yb:KLuF₄ in water as well. A homebuilt laser trapping instrument illustrated in Figure 4a was used to measure the temperature of an individual 10% Yb:KLuF₄ microcrystal through analysis of the particle's cold Brownian motion at a trapping wavelength of $\lambda = 1020$ nm. To minimize heating of the trapping chamber, the microcrystals were trapped at a distance of 40 μ m away from the quartz substrate, approximately in the middle of the fluid chamber. The dynamics of a trapped particle were observed by recording the forward-scattered laser light via a quadrant photodiode (QPD). A power spectral density (PSD) vs frequency plot (Figure 4b) was generated by performing the Fourier transform. The temperature was extracted from the PSD by the established method in refs 24, 25. In brief, a 32 Hz oscillation of the trapping chamber was driven by the piezostage to convert the photovoltage signal in units of volts to units of length [m]. The local temperature of the trapped 10% Yb:KLuF₄ microcrystal and surrounding water decreased 7.2 ± 0.6 K below room temperature, as shown in Figure 4c. As a control, we also measured the temperature of the same 10% Yb:KLuF₄ microcrystal trapped in water with a 1064 nm laser,

which is not resonant with Yb³⁺ absorption but can heat the surrounding water. With the same temperature extraction method, the sample temperature increased above 50°C. Optical trapping experiments with the 10%Yb:K₂LuF₅ phase showed reduced heating in water as evidenced by stable temperature with increased irradiance (Figure S12).

Although net cooling was not observed with pulverized 10% Yb:K₂LuF₅ materials in water, cooling was observed in vacuum with nonground, 30 μ m long crystals with unbroken surfaces (Figure \$13). Surface defects could be the reason for different cooling performances of these different KLF phases. Small crystals with large surface-to-volume ratios have large nonradiative losses, especially for the KLu₃F₁₀ nanoparticles, which shows a short luminescence lifetime. Besides the size effect, the higher maximal phonon energies of KLu₃F₁₀ (509 cm⁻¹) and KLu₂F₇ (529 cm⁻¹) than those of KLuF₄ (508 cm⁻¹) and K_2LuF_5 (506 cm⁻¹) also facilitate nonradiative relaxation. It is noted that all K-Lu-F phases have higher maximal phonon energies than other laser cooling materials, although they are rather low phonon energy fluorides. However, they still have long Yb^{3+ 2} $F_{5/2}$ lifetimes, which indicate high purity of these crystals and low nonradiative loss for laser cooling. The PL line width and site homogeneity are also important for laser refrigeration. Future work will focus on low-temperature spectroscopic studies of these materials and also the growth of larger crystal grains from KLu₃F₁₀ and KLu₂F₇ phases.

CONCLUSIONS

Potassium lutetium fluoride is a relatively unexplored member of the alkali-RE-fluoride family for solid-state laser refrigeration. It has several crystallographic polymorphs with various KF/LuF₃ binary compound ratios, providing a rich array of potential host environments for Yb³+ ions. In this article, we present the low-cost, rapid hydrothermal synthesis of four distinct phases of KLF nano- or microcrystals with the general stoichiometric formula (KF) $_x$ ·(LuF₃) $_y$, including KLuF₄ (trigonal), KLu₂F₇ (orthorhombic), KLu₃F₁₀ (cubic), and K₂LuF₅ (orthorhombic). Each phase was doped with 10% ytterbium ions, and two of these phases (KLuF₄ and K₂LuF₅) were observed to be viable candidates for solid-state laser refrigeration. This is the first experimental report of laser

cooling for $\mathrm{KLuF_4}$ grown through hydrothermal synthesis. It is also the first experimental report of laser cooling of the $\mathrm{K_2LuF_5}$ phase grown through any synthetic method. Luminescence spectra and lifetimes of the four crystalline phases were characterized and interpreted based on the point-group symmetry of the trivalent cations in each crystal phase. Laser refrigeration was demonstrated using both optomechanical cantilevers in vacuum and also through observing the Brownian dynamics of the crystals optically trapped in water. Yb: $\mathrm{KLuF_4}$ shows the most significant cooling, with minimum temperatures 8.6 \pm 2.1 K below room temperature. Each crystalline phase exhibits distinct morphologies that may be advantageous in the future development of radiation-balanced microlasers.

■ EXPERIMENTAL SECTION

KLF Synthesis. Lutetium nitrate (Lu(NO₃)₃) and ytterbium nitrate (Yb(NO₃)₃) were of 99.99% purity and purchased from Sigma-Aldrich. Potassium hydroxide (KOH), potassium fluoride (KF), ethanol, and oleic acid were analytical grade purchased from Sigma-Aldrich and used without further purification. Milli-Q deionized water (18.2 M Ω × cm) was used for each synthesis. For a typical synthesis, 420.8 mg of KOH was dissolved in 1.5 mL of water, followed by 5 mL of ethanol and 5 mL of oleic acid with stirring. Then, 1.44 mL of 0.5M Lu(NO₃)₃ and 0.16 mL of 0.5 M Yb(NO₃)₃ were added to the mixture. After stirring for 10 min, 3 mL of aqueous KF solution was added dropwise. The molar concentration of the KF solution depends on the target product. After additional agitation for 10 min, the resulting mixture was transferred to a 23 mL Teflon-lined autoclave and heated at 220 °C for 24 h. After the autoclave cooled to room temperature, crystals were isolated by washing and centrifuging by ethanol and water three times. After drying the product at 60 °C for 12 h, they were transferred to a Lindberg Blue tube furnace and heated at 300 $^{\circ}\text{C}$ for 2 h to remove the organic surface ligand.

Powder X-ray Diffraction (XRD). XRD patterns were obtained on a Bruker F8 Focus Powder XRD with Cu K (40 kV, 40 mA) irradiation ($\lambda = 0.154$ nm). The 2θ angle of the XRD data is from 10 to 60° , and the scanning rate was 0.36° s⁻¹.

PL Measurement. A 1020 nm laser from a fiber-coupled single-mode laser diode (QPhotonics, QFBGLD-1020-400) was focused to a diffraction-limited spot (radius = 1.2 μ m) using a long working distance 50× objective (Mitutoyo, M Plan Apo), and PL was collected by the same objective. The PL spectra were recorded with an Acton SpectraPro 500i spectrograph with a Princeton liquid-nitrogen-cooled Si detector. A 1000 nm short-pass filter (Thorlabs, FESH1000) was used to filter the laser line. Ten spectra, collected for 10 ms each, were averaged to obtain the final PL spectrum.

Time-Gated Full Yb PL Measurement. A Tektronics function generator was used to control the laser diode and generate laser pulses of a 2 ms duration with a frequency of 10 Hz. A second channel of the function generator was used to control the shutter in the spectrometer. The shutter open time was set to 20 ms with the same frequency of the laser. The phase between the two signals was tuned to let the shutter open in the luminescence decay regime but eliminate the scattered laser light. A full-wavelength spectrum including the laser excitation wavelength range could be recorded without applying the short-pass filter.

Luminescence Lifetime Measurement. The same function generator was used to generate a 1 ms pulse. An avalanche photodiode (APD) detector (Thorlabs APD430A) was used to collect the luminescence decay signal.

Eigenfrequency Measurement. A nanomanipulator (Märzhäuser-Wetzlär) with a tungsten dissecting probe (World Precision Instruments, 100 nm) was used to transfer the CdSNR to a silicon wafer. The hydrothermal product was ground into small pieces with a mortar and pestle. Then, a ground piece of 10%Yb:KLuF₄ crystal was transferred to the free end of the cantilever. The silicon substrate

loaded with the CdSNR cantilever and the crystal sample was then attached via a copper tape to the stage of an optical cryostat (Janis ST-500). The chamber was pumped down to a pressure of 4.0×10^{-4} mbar. Forward-scattered laser radiation was collected with the APD from behind the chamber (Figure 3a). Ten power spectra were averaged to obtain one measurement, as shown in Figure 3c. The peak then was fit to a Lorentzian profile to obtain the cantilever's eigenfrequency. Temperature calibration was performed by heating the cryostat using a temperature controller (Lake Shore 335, resolution: 10 mK) and measuring the eigenfrequency of the cantilever at different temperatures using a low laser irradiance (0.1 MW cm⁻²). For each measurement, an average frequency data point was obtained by fitting six measurements obtained at the same laser power with a gap of 1 min between consecutive measurements. The error bars represent 1 standard deviation.

Laser Trapping and Temperature Extraction. The laser-tweezer setup was modified based on a modular optical tweezer kit (Thorlabs, OTKB), 25 where the original condenser lens was replaced with a 10× Mitutoyo condenser (Plan Apo infinity-corrected long WD objective). The laser was focused by a 100× objective lens (Nikon) to 1.1 μ m. The trapping chamber was a glass slide and coverslip spaced by a double-sided tape (EMS) of 150 μ m thickness. Microcrystals were trapped at the center (30–40 μ m from the surface) of the chamber. The particle Brownian motion traces were collected by the condenser and recorded by a quadric photodiode (QPD). The methods for data processing and temperature extraction can be found in refs24, 25.

ASSOCIATED CONTENT

Supporting Information

The Supporting Information is available free of charge at https://pubs.acs.org/doi/10.1021/acs.chemmater.1c00420.

Experimental procedures and characterization data for all samples including time-series XRD, optical microscopic images, ATR-FTIR spectra, cantilever eigenfrequency measurement, optical trapping, mean luminescence wavelength measurement; and discussion about potential growth mechanisms and crystal growth velocities (PDF)

AUTHOR INFORMATION

Corresponding Author

Peter J. Pauzauskie — Department of Materials Science & Engineering, University of Washington, Seattle, Washington 98195, United States; Physical & Computational Sciences Directorate, Pacific Northwest National Laboratory, Richland, Washington 99352, United States; oorcid.org/0000-0002-1554-5949; Email: peterpz@uw.edu

Authors

Xiaojing Xia — Molecular Engineering & Science Institute, University of Washington, Seattle, Washington 98195, United States; © orcid.org/0000-0003-2713-6891

Anupum Pant – Department of Materials Science & Engineering, University of Washington, Seattle, Washington 98195, United States; oorcid.org/0000-0002-6253-8418

Xuezhe Zhou — Department of Materials Science & Engineering, University of Washington, Seattle, Washington 98195, United States

Elena A. Dobretsova — Department of Materials Science & Engineering, University of Washington, Seattle, Washington 98195, United States; Present Address: Prokhorov General Physics Institute of the Russian Academy of Sciences, Moscow 119991, Russia.; orcid.org/0000-0001-6153-3845

- Alexander B. Bard Department of Chemistry, University of Washington, Seattle, Washington 98195, United States;
 orcid.org/0000-0002-9000-3277
- Matthew B. Lim Department of Materials Science & Engineering, University of Washington, Seattle, Washington 98195, United States
- Joo Yeon D. Roh Department of Chemistry, University of Washington, Seattle, Washington 98195, United States;
 orcid.org/0000-0001-9801-3069
- Daniel R. Gamelin Department of Chemistry, University of Washington, Seattle, Washington 98195, United States;
 ocid.org/0000-0003-2888-9916

Complete contact information is available at: https://pubs.acs.org/10.1021/acs.chemmater.1c00420

Notes

The authors declare no competing financial interest.

ACKNOWLEDGMENTS

X.X., A.P., and P.J.P. acknowledge support from the MURI:MARBLe project under the auspices of the Air Force Office of Scientific Research (Award #FA9550-16-1-0362). This research was partially supported by the National Science Foundation (NSF) through the UW Molecular Engineering Materials Center, a Materials Research Science and Engineering Center (DMR-1719797 to D.R.G. and P.J.P.). A.B.B. and P.J.P. acknowledge support from the U.S. Department of Energy, Office of Science (DOE), Basic Energy Sciences (BES), Division of Materials Sciences and Engineering at the University of Washington (UW) and the Pacific Northwest National Laboratory (PNNL) for TEM and SEM characterizations. PNNL is a multiprogram national laboratory operated for DOE by Battelle under Contract No. DE-AC05-76RL01830. All authors acknowledge support from the UW Nano-engineered systems institute. Part of this work was conducted at the Molecular Analysis Facility, a National Nanotechnology Coordinated Infrastructure site at the University of Washington, which is supported, in part, by the National Science Foundation (grant NNCI-1542101), the University of Washington, the Molecular Engineering Sciences Institute, and the Clean Energy Institute. The authors acknowledge N.N. Novikova and S.A. Klimin for their assistance in ATR-FTIR measurements.

REFERENCES

- (1) Kumar, R.; Nyk, M.; Ohulchanskyy, T. Y.; Flask, C. A.; Prasad, P. N. Combined Optical and MR Bioimaging Using Rare Earth Ion Doped NaYF₄ Nanocrystals. *Adv. Funct. Mater.* **2009**, *19*, 853–859.
- (2) Xu, A.-W.; Gao, Y.; Liu, H.-Q. The Preparation, Characterization, and Their Photocatalytic Activities of Rare-Earth-Doped TiO₂ Nanoparticles. *J. Catal.* **2002**, *207*, 151–157.
- (3) Wang, H.-Q.; Batentschuk, M.; Osvet, A.; Pinna, L.; Brabec, C. J. Rare-Earth Ion Doped Up-Conversion Materials for Photovoltaic Applications. *Adv. Mater.* **2011**, 23, 2675–2680.
- (4) Serrano, D.; Braud, A.; Doualan, J. L.; Camy, P.; Benayad, A.; Ménard, V.; Moncorgé, R. Ytterbium Sensitization in KY₃F₁₀: Pr³⁺, Yb³⁺ for Silicon Solar cells Efficiency Enhancement. *Opt. Mater.* **2011**, 33, 1028–1031.
- (5) Crane, M. J.; Kroupa, D. M.; Gamelin, D. R. Detailed-Balance Analysis of Yb³⁺:CsPb(Cl_{1-x}Br_x)₃ Quantum-Cutting Layers for High-Efficiency Photovoltaics under Real-World Conditions. *Energy Environ. Sci.* **2019**, *12*, 2486–2495.

- (6) Bünzli, J.-C. G.; Eliseeva, S. V. Lanthanide NIR Luminescence for Telecommunications, Bioanalyses and Solar Energy Conversion. *J. Rare Earths* **2010**, 28, 824–842.
- (7) Thiel, C. W.; Böttger, T.; Cone, R. L. Rare-Earth-Doped Materials for Applications in Quantum Information Storage and Signal Processing. *J. Lumin.* **2011**, *131*, 353–361.
- (8) Xia, X.; Pant, A.; Ganas, A. S.; Jelezko, F.; Pauzauskie, P. J. Quantum Point Defects for Solid-State Laser Refrigeration. *Adv. Mater.* **2020**, No. 1905406.
- (9) Pringsheim, P. Zwei Bemerkungen über den Unterschied von Lumineszenz- und Temperaturstrahlung. Z. Phys. **1929**, 57, 739–746.
- (10) Kastler, A. Quelques suggestions concernant la production optique et la détection optique d'une inégalité de population des niveaux de quantifigation spatiale des atomes. Application à l'expérience de Stern et Gerlach et à la résonance magnétique. *J. Phys. Radium* **1950**, *11*, 255–265.
- (11) Epstein, R. I.; Buchwald, M. I.; Edwards, B. C.; Gosnell, T. R.; Mungan, C. E. Observation of Laser-Induced Fluorescent Cooling of a Solid. *Nature* 1995, 377, 500–503.
- (12) Rayner, A.; Friese, M. E. J.; Truscott, A. G.; Heckenberg, N. R.; Rubinsztein-Dunlop, H. Laser Cooling of a Solid from Ambient Temperature. *J. Mod. Opt.* **2001**, *48*, 103–114.
- (13) Hoyt, C. W.; Sheik-Bahae, M.; Epstein, R. I.; Edwards, B. C.; Anderson, J. E. Observation of Anti-Stokes Fluorescence Cooling in Thulium-Doped Glass. *Phys. Rev. Lett.* **2000**, *85*, 3600–3603.
- (14) Fernández, J.; Mendioroz, A.; García, A.; Balda, R.; Adam, J. Anti-Stokes Laser-Induced Internal Cooling of Yb-doped Glasses. *Phys. Rev. B: Condens. Matter Mater. Phys.* **2000**, *62*, 3213–3217.
- (15) Fernandez, J.; Garcia-Adeva, A. J.; Balda, R. Anti-Stokes Laser Cooling in Bulk Erbium-Doped Materials. *Phys. Rev. Lett.* **2006**, *97*, No. 033001.
- (16) Mobini, E.; Rostami, S.; Peysokhan, M.; Albrecht, A.; Kuhn, S.; Hein, S.; Hupel, C.; Nold, J.; Haarlammert, N.; Schreiber, T.; et al. Laser cooling of ytterbium-doped silica glass. *Commun. Phys.* **2020**, 3, No. 134.
- (17) Epstein, R. I.; Brown, J. J.; Edwards, B. C.; Gibbs, A. Measurements of Optical Refrigeration in Ytterbium-Doped Crystals. *J. Appl. Phys.* **2001**, *90*, 4815–4819.
- (18) Mendioroz, A.; Fernández, J.; Voda, M.; Al-Saleh, M.; Balda, R.; García-Adeva, A. J. Anti-Stokes Laser Cooling in Yb^{3+} -Doped KPb_2Cl_5 Crystal. *Opt. Lett.* **2002**, *27*, 1525.
- (19) Rostami, S.; Albrecht, A. R.; Volpi, A.; Hehlen, M. P.; Tonelli, M.; Sheik-Bahae, M. Tm-doped Crystals for Mid-IR Optical Cryocoolers and Radiation Balanced Lasers. *Opt. Lett.* **2019**, *44*, 1419–1422.
- (20) Volpi, A.; Cittadino, G.; Di Lieto, A.; Tonelli, M. Anti-Stokes Cooling of Yb-doped KYF₄ Single Crystals. *J. Lumin.* **2018**, 203, 670–675.
- (21) Volpi, A.; Krämer, K. W.; Biner, D.; Wiggins, B.; Kock, J.; Albrecht, A. R.; Peterson, E. J.; Spilde, M. N.; Sheik-Bahae, M.; Hehlen, M. P. Bridgman Growth of Laser-Cooling-Grade LiLuF₄: Yb³⁺ Single. *Cryst. Growth Des.* **2021**, *21*, 2142–2153.
- (22) Sheik-Bahae, M.; Epstein, R. I. Optical Refrigeration. *Nat. Photonics* **2007**, *1*, 693–699.
- (23) Melgaard, S. D.; Albrecht, A. R.; Hehlen, M. P.; Sheik-Bahae, M. Solid-State Optical Refrigeration to Sub-100 Kelvin Regime. *Sci. Rep.* **2016**, *6*, No. 20380.
- (24) Roder, P. B.; Smith, B. E.; Zhou, X.; Crane, M. J.; Pauzauskie, P. J. Laser Refrigeration of Hydrothermal Nanocrystals in Physiological Media. *Proc. Natl. Acad. Sci. U.S.A.* **2015**, *112*, 15024–15029.
- (25) Zhou, X.; Smith, B. E.; Roder, P. B.; Pauzauskie, P. J. Laser Refrigeration of Ytterbium-Doped Sodium-Yttrium-Fluoride Nanowires. *Adv. Mater.* **2016**, *28*, 8658–8662.
- (26) Chai, B. H. T.; Lefaucheur, J.; Pham, A.-T.; Loutts, G. B.; Nicholls, J. F. Growth of High-Quality Single Crystals of KYF₄ by TSSG Method, in *Growth, Characterization, and Applications of Laser Host and Nonlinear Crystals II*, Proceedings of International Society for Optics and Photonics, 1993, pp 131 135.

- (27) Levin, E. M.; McMurdie, H. Phase Diagrams for Ceramists, 1975 Supplement; American Ceramic Society, Inc.: Columbus, 1975; p 515.
- (28) Fedorov, P. Systems of alkali and rare-earth metal fluorides. Russ. J. Inorg. Chem. 1999, 44, 1703–1727.
- (29) Cao, C.; Guo, S.; Moon, B. K.; Choi, B. C.; Jeong, J. H. Synthesis, grouping, and optical properties of REF₃-KF nanocrystals. *Mater. Chem. Phys.* **2013**, *139*, 609–615.
- (30) Hehlen, M. P. Crystal-Field Effects in Fluoride Crystals for Optical Refrigeration. Proceedings of SPIE 7614, Laser Refrigeration of Solids III, 2010, p 761404.
- (31) Bukhalova, G.; Bahaeva, E.; TM, K. Phase Diagrams for Ceramists. Zh. Neorg. Khim. 1965, 10, 2127-2131.
- (32) Jia, Y. Crystal Radii and Effective Ionic Radii of the Rare Earth Ions. J. Solid State Chem. 1991, 95, 184–187.
- (33) Pant, A.; Xia, X.; Davis, E. J.; Pauzauskie, P. J. Solid-state laser refrigeration of a composite semiconductor Yb: YLiF 4 optomechanical resonator. *Nat. Commun.* **2020**, *11*, No. 3235.
- (34) Seletskiy, D. V.; Melgaard, S. D.; Epstein, R. I.; Di Lieto, A.; Tonelli, M.; Sheik-Bahae, M. Precise determination of minimum achievable temperature for solid-state optical refrigeration. *J. Lumin.* **2013**, *133*, 5–9.
- (35) Bowman, S.; O'Connor, S.; Biswal, S. Radiation Balanced Lasers, 2005 Conference on Lasers and Electro-Optics Europe; CLEO: Europe, 2005; pp 35.
- (36) Ding, M.; Zhu, F.; Ma, D.; Huang, X.; Liu, P.; Song, K.; Zhong, J.; Xi, J.; Ji, Z.; Chen, D. KF-Mediated Controlled-Synthesis of Potassium Ytterbium Fluorides (Doped with Er³⁺) with Phase-Dependent Upconversion Luminescence. *CrystEngComm* **2015**, *17*, 7182–7190.
- (37) Zhong, B.; Yin, J.; Jia, Y.; Chen, L.; Hang, Y.; Yin, J. Laser Cooling of Yb³⁺-doped LuLiF₄ crystal. *Opt. Lett.* **2014**, 39, 2747–2750.
- (38) Bard, A. B.; Zhou, X.; Xia, X.; Zhu, G.; Lim, M. B.; Kim, S. M.; Johnson, M. C.; Kollman, J. M.; Marcus, M. A.; Spurgeon, S. R.; et al. A Mechanistic Understanding of Nonclassical Crystal Growth in Hydrothermally Synthesized Sodium Yttrium Fluoride Nanowires. *Chem. Mater.* **2020**, *32*, 2753–2763.
- (39) Wu, H.; Hao, Z.; Zhang, L.; Zhang, X.; Xiao, Y.; Pan, G. H.; Wu, H.; Luo, Y.; Zhao, H.; Zhang, J. Phonon Energy Dependent Energy Transfer Upconversion for the Red Emission in the Er³⁺/Yb³⁺ System. *J. Phys. Chem. C* **2018**, *122*, 9611–9618.
- (40) Grzechnik, A.; Bouvier, P.; Mezouar, M.; Mathews, M.; Tyagi, A.; Köhler, J. Hexagonal $Na_{1.5}Y_{1.5}F_6$ at high pressures. *J. Solid State Chem.* **2002**, *165*, 159–164.
- (41) Wang, X.; Li, Y. Synthesis and Characterization of Lanthanide Hydroxide Single-Crystal Nanowires. *Angew. Chem., Int. Ed.* **2002**, *41*, 4790–4793.
- (42) Karbowiak, M.; Gnutek, P.; Rudowicz, C. Energy Levels and Crystal Field Parameters for Nd³⁺ Ions in BaY₂F₈, LiKYF₅, and K₂YF₅ Single Crystals. *Spectrochim. Acta, Part A* **2012**, 87, 46–60.
- (43) Henderson, B.; Bartram, R. H. *Crystal-Field Engineering of Solid-State Laser Materials*; Cambridge University Press: Cambridge, 2000; pp 30–60, 253–300.
- (44) Zhou, X.; Xia, X.; Smith, B. E.; Lim, M. B.; Bard, A. B.; Pant, A.; Pauzauskie, P. J. Interface-Dependent Radiative Lifetimes of Yb³⁺, Er³⁺ Co-Doped Single NaYF₄ Upconversion Nanowires. *ACS Appl. Mater. Interfaces* **2019**, *11*, 22817–22823.
- (45) Saha, S.; Chowdhury, P. S.; Patra, A. Luminescence of Ce³⁺ in Y₂SiO₅ Nanocrystals: Role of Crystal Structure and Crystal Size. *J. Phys. Chem. B* **2005**, *109*, 2699–2702.
- (46) Eichhorn, M. Fluorescence Reabsorption and Its Effects on the Local Effective Excitation Lifetime. *Appl. Phys. B* **2009**, *96*, 369–377.
- (47) Xue, X.; Uechi, S.; Tiwari, R. N.; Duan, Z.; Liao, M.; Yoshimura, M.; Suzuki, T.; Ohishi, Y. Size-Dependent Upconversion Luminescence and Quenching Mechanism of LiYF₄: Er³⁺/Yb³⁺ Nanocrystals with Oleate Ligand Adsorbed. *Opt. Mater. Express* **2013**, *3*, 989.

- (48) Sumida, D. S.; Fan, T. Y. Effect of Radiation Trapping on Fluorescence Lifetime and Emission Cross Section Measurements in Solid-State Laser Media. *Opt. Lett.* **1994**, *19*, 1343.
- (49) Pant, A.; Smith, B. E.; Crane, M. J.; Zhou, X.; Lim, M. B.; Frazier, S. A.; Davis, E. J.; Pauzauskie, P. J. Optomechanical Thermometry of Nanoribbon Cantilevers. *J. Phys. Chem. C* **2018**, 122, 7525–7532.